# Measurement of inelastic J/ψ production in deep inelastic scattering at HERA

ZEUS Collaboration

Abstract

The inelastic production of J/ψ mesons in ep collisions has been studied with the ZEUS detector at HERA using an integrated luminosity of $109\,\mathrm{pb}^{-1}$. The J/ψ mesons were identified using the decay channel $J/\psi \to \mu^+\mu^-$. The measurements were performed in the kinematic range $2 < Q^2 < 80\,\mathrm{GeV}^2$, $50 < W < 250\,\mathrm{GeV}$, $0.2 < z < 0.9$ and $-1.6 < Y_{\mathrm{lab}} < 1.3$, where Q^2 is the virtuality of the exchanged photon, W is the photon–proton centre–of–mass energy, z is the fraction of the photon energy carried by the J/ψ meson in the proton rest frame and Y_{lab} is the rapidity of the J/ψ in the laboratory frame. The measured cross sections are compared to theoretical predictions within the non-relativistic QCD framework including colour–singlet and colour–octet contributions, as well as to predictions based on the k_T–factorisation approach. Calculations of the colour–singlet process generally agree with the data, whereas inclusion of colour–octet terms spoils this agreement.
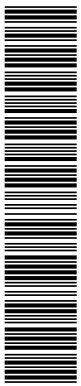
The ZEUS Collaboration

S. Chekanov, M. Derrick, S. Magill, S. Miglioranzi[1], B. Musgrave, J. Repond, R. Yoshida
Argonne National Laboratory, Argonne, Illinois 60439-4815, USA [n]

M.C.K. Mattingly
Andrews University, Berrien Springs, Michigan 49104-0380, USA

N. Pavel, A.G. Yagües Molina
Institut für Physik der Humboldt-Universität zu Berlin, Berlin, Germany

P. Antonioli, G. Bari, M. Basile, L. Bellagamba, D. Boscherini, A. Bruni, G. Bruni, G. Cara Romeo, L. Cifarelli, F. Cindolo, A. Contin, M. Corradi, S. De Pasquale, P. Giusti, G. Iacobucci, A. Margotti, A. Montanari, R. Nania, F. Palmonari, A. Pesci, A. Polini, L. Rinaldi, G. Sartorelli, A. Zichichi
University and INFN Bologna, Bologna, Italy [e]

G. Aghuzumtsyan, D. Bartsch, I. Brock, S. Goers, H. Hartmann, E. Hilger, P. Irrgang, H.-P. Jakob, O.M. Kind, U. Meyer, E. Paul[2], J. Rautenberg, R. Renner, K.C. Voss[3], M. Wang, M. Wlasenko
Physikalisches Institut der Universität Bonn, Bonn, Germany [b]

D.S. Bailey[4], N.H. Brook, J.E. Cole, G.P. Heath, T. Namsoo, S. Robins
H.H. Wills Physics Laboratory, University of Bristol, Bristol, United Kingdom [m]

M. Capua, S. Fazio, A. Mastroberardino, M. Schioppa, G. Susinno, E. Tassi
Calabria University, Physics Department and INFN, Cosenza, Italy [e]

J.Y. Kim, K.J. Ma[5]
Chonnam National University, Kwangju, South Korea [g]

M. Helbich, Y. Ning, Z. Ren, W.B. Schmidke, F. Sciulli
Nevis Laboratories, Columbia University, Irvington on Hudson, New York 10027 [o]

J. Chwastowski, A. Eskreys, J. Figiel, A. Galas, K. Olkiewicz, P. Stopa, D. Szuba, L. Zawiejski
Institute of Nuclear Physics, Cracow, Poland [i]

L. Adamczyk, T. Bołd, I. Grabowska-Bołd, D. Kisielewska, J. Łukasik, M. Przybycień, L. Suszycki, J. Szuba[6]
Faculty of Physics and Applied Computer Science, AGH-University of Science and Technology, Cracow, Poland [p]

A. Kotański[7], W. Słomiński
Department of Physics, Jagellonian University, Cracow, Poland

V. Adler, U. Behrens, I. Bloch, K. Borras, G. Drews, J. Fourletova, A. Geiser, D. Gladkov, P. Göttlicher[8], O. Gutsche, T. Haas, W. Hain, C. Horn, B. Kahle, U. Kötz, H. Kowalski, G. Kramberger, H. Lim, B. Löhr, R. Mankel, I.-A. Melzer-Pellmann, C.N. Nguyen, D. Notz, A.E. Nuncio-Quiroz, A. Raval, R. Santamarta, U. Schneekloth, H. Stadie, U. Stösslein, G. Wolf, C. Youngman, W. Zeuner
Deutsches Elektronen-Synchrotron DESY, Hamburg, Germany

S. Schlenstedt
Deutsches Elektronen-Synchrotron DESY, Zeuthen, Germany

G. Barbagli, E. Gallo, C. Genta, P. G. Pelfer
University and INFN, Florence, Italy [e]

A. Bamberger, A. Benen, F. Karstens, D. Dobur, N.N. Vlasov[9]
Fakultät für Physik der Universität Freiburg i.Br., Freiburg i.Br., Germany [b]

P.J. Bussey, A.T. Doyle, W. Dunne, J. Ferrando, J. Hamilton, D.H. Saxon, I.O. Skillicorn
Department of Physics and Astronomy, University of Glasgow, Glasgow, United Kingdom [m]

I. Gialas[10]
Department of Engineering in Management and Finance, Univ. of Aegean, Greece

T. Carli[11], T. Gosau, U. Holm, N. Krumnack[12], E. Lohrmann, M. Milite, H. Salehi, P. Schleper, T. Schörner-Sadenius, S. Stonjek[13], K. Wichmann, K. Wick, A. Ziegler, Ar. Ziegler
Hamburg University, Institute of Exp. Physics, Hamburg, Germany [b]

C. Collins-Tooth[14], C. Foudas, C. Fry, R. Gonçalo[15], K.R. Long, A.D. Tapper
Imperial College London, High Energy Nuclear Physics Group, London, United Kingdom [m]

M. Kataoka[16], K. Nagano, K. Tokushuku[17], S. Yamada, Y. Yamazaki
Institute of Particle and Nuclear Studies, KEK, Tsukuba, Japan [f]

A.N. Barakbaev, E.G. Boos, N.S. Pokrovskiy, B.O. Zhautykov
Institute of Physics and Technology of Ministry of Education and Science of Kazakhstan, Almaty, Kazakhstan

D. Son
Kyungpook National University, Center for High Energy Physics, Daegu, South Korea [g]

J. de Favereau, K. Piotrzkowski
Institut de Physique Nucléaire, Université Catholique de Louvain, Louvain-la-Neuve, Belgium [q]

F. Barreiro, C. Glasman[18], M. Jimenez, L. Labarga, J. del Peso, J. Terrón, M. Zambrana
Departamento de Física Teórica, Universidad Autónoma de Madrid, Madrid, Spain [l]

F. Corriveau, C. Liu, M. Plamondon, A. Robichaud-Veronneau, R. Walsh, C. Zhou
Department of Physics, McGill University, Montréal, Québec, Canada H3A 2T8 [a]

T. Tsurugai
Meiji Gakuin University, Faculty of General Education, Yokohama, Japan [f]

A. Antonov, B.A. Dolgoshein, I. Rubinsky, V. Sosnovtsev, A. Stifutkin, S. Suchkov
Moscow Engineering Physics Institute, Moscow, Russia [j]

R.K. Dementiev, P.F. Ermolov, L.K. Gladilin, I.I. Katkov, L.A. Khein, I.A. Korzhavina, V.A. Kuzmin, B.B. Levchenko, O.Yu. Lukina, A.S. Proskuryakov, L.M. Shcheglova, D.S. Zotkin, S.A. Zotkin
Moscow State University, Institute of Nuclear Physics, Moscow, Russia [k]

I. Abt, C. Büttner, A. Caldwell, X. Liu, J. Sutiak
Max-Planck-Institut für Physik, München, Germany

N. Coppola, G. Grigorescu, A. Keramidas, E. Koffeman, P. Kooijman, E. Maddox, H. Tiecke, M. Vázquez, L. Wiggers
NIKHEF and University of Amsterdam, Amsterdam, Netherlands [h]

N. Brümmer, B. Bylsma, L.S. Durkin, T.Y. Ling
Physics Department, Ohio State University, Columbus, Ohio 43210 [n]

P.D. Allfrey, M.A. Bell, A.M. Cooper-Sarkar, A. Cottrell, R.C.E. Devenish, B. Foster, C. Gwenlan[19], T. Kohno, K. Korcsak-Gorzo, S. Patel, P.B. Straub, R. Walczak
Department of Physics, University of Oxford, Oxford United Kingdom [m]

P. Bellan, A. Bertolin, R. Brugnera, R. Carlin, R. Ciesielski, F. Dal Corso, S. Dusini, A. Garfagnini, S. Limentani, A. Longhin, L. Stanco, M. Turcato
Dipartimento di Fisica dell' Università and INFN, Padova, Italy [e]

E.A. Heaphy, F. Metlica, B.Y. Oh, J.J. Whitmore[20]
Department of Physics, Pennsylvania State University, University Park, Pennsylvania 16802 [o]

Y. Iga
Polytechnic University, Sagamihara, Japan [f]

G. D'Agostini, G. Marini, A. Nigro
Dipartimento di Fisica, Università 'La Sapienza' and INFN, Rome, Italy [e]

J.C. Hart
Rutherford Appleton Laboratory, Chilton, Didcot, Oxon, United Kingdom [m]

H. Abramowicz[21], A. Gabareen, S. Kananov, A. Kreisel, A. Levy
Raymond and Beverly Sackler Faculty of Exact Sciences, School of Physics, Tel-Aviv University, Tel-Aviv, Israel [d]

M. Kuze
Department of Physics, Tokyo Institute of Technology, Tokyo, Japan [f]

S. Kagawa, T. Tawara
Department of Physics, University of Tokyo, Tokyo, Japan [f]

R. Hamatsu, H. Kaji, S. Kitamura[22], K. Matsuzawa, O. Ota, Y.D. Ri
Tokyo Metropolitan University, Department of Physics, Tokyo, Japan [f]

M. Costa, M.I. Ferrero, V. Monaco, R. Sacchi, A. Solano
Università di Torino and INFN, Torino, Italy [e]

M. Arneodo, M. Ruspa
Università del Piemonte Orientale, Novara, and INFN, Torino, Italy [e]

S. Fourletov, J.F. Martin
Department of Physics, University of Toronto, Toronto, Ontario, Canada M5S 1A7 [a]

J.M. Butterworth[23], R. Hall-Wilton, T.W. Jones, J.H. Loizides[24], M.R. Sutton[4], C. Targett-Adams, M. Wing
Physics and Astronomy Department, University College London, London, United Kingdom [m]

J. Ciborowski[25], G. Grzelak, P. Kulinski, P. Łużniak[26], J. Malka[26], R.J. Nowak, J.M. Pawlak, J. Sztuk[27], T. Tymieniecka, A. Tyszkiewicz[26], A. Ukleja, J. Ukleja[28], A.F. Żarnecki
Warsaw University, Institute of Experimental Physics, Warsaw, Poland

M. Adamus, P. Plucinski
Institute for Nuclear Studies, Warsaw, Poland

Y. Eisenberg, D. Hochman, U. Karshon, M.S. Lightwood
Department of Particle Physics, Weizmann Institute, Rehovot, Israel [c]

E. Brownson, T. Danielson, A. Everett, D. Kçira, S. Lammers, L. Li, D.D. Reeder, M. Rosin, P. Ryan, A.A. Savin, W.H. Smith
Department of Physics, University of Wisconsin, Madison, Wisconsin 53706, USA [n]

S. Dhawan
Department of Physics, Yale University, New Haven, Connecticut 06520-8121, USA [n]

S. Bhadra, C.D. Catterall, Y. Cui, G. Hartner, S. Menary, U. Noor, M. Soares, J. Standage, J. Whyte
Department of Physics, York University, Ontario, Canada M3J 1P3 [a]

VI

1 Introduction

Inelastic production of charmonium can be described in two steps. The first step is the creation of a $c\bar{c}$ quark pair, a process which can be calculated in perturbative Quantum Chromodynamics (QCD). The second step is the formation of the J/ψ bound state, which occurs at long distances and is described by phenomenological models.

When charmonium production was first investigated at CERN [1] and Fermilab [2] it was hoped that the production cross section could be used to determine the gluon density in the proton, because the gluon density directly enters the cross–section calculation. This idea was encouraged by the qualitative agreement of the data with the predictions of LO QCD within the framework of the colour–singlet model (CSM) [3] in which the $c\bar{c}$ pair is formed in a CS state identified with the J/ψ. Later data from $p\bar{p}$ collisions at Fermilab [4] indicated that the CSM is not able to describe J/ψ production at large J/ψ transverse momenta, and hence that there may be significant contributions from higher orders in QCD or from the production of $c\bar{c}$ pairs in colour–octet (CO) states, which evolve into J/ψ mesons via radiation of soft gluons.

Models have been developed in the framework of non-relativistic QCD (NRQCD) [5] in which CS and CO contributions coexist. The transition of the coloured $c\bar{c}$ pair, with a given angular momentum, into a J/ψ is described in terms of long–distance matrix elements tuned to experimental data (hadroproduction of J/ψ mesons or B–meson decays to J/ψ). As well as describing high–p_T charmonium production in $p\bar{p}$ collisions [4], NRQCD calculations including CS and CO contributions are also consistent with the data on production of J/ψ mesons in $\gamma\gamma$ interactions at LEP2 [6]. However, J/ψ polarisation data from CDF [7] are inconsistent with NRQCD predictions. Comparisons with the decay angular distributions measured in e^+e^- collisions at BaBar [8] and Belle [9] are inconclusive.

The production of J/ψ mesons in ep collisions at HERA is sensitive to both CS and CO contributions. The CS mechanism is expected to be the dominant contribution at intermediate values of the inelasticity variable, $z \lesssim 0.7$. In the proton rest frame, z is the fraction of the virtual photon energy transferred to the J/ψ. The CO mechanism is expected to be dominant at high z. However, large contributions from the elastic and diffractive proton–dissociative J/ψ production processes [10,11] are also present at $z \approx 1$.

Inelastic J/ψ production at HERA was studied previously in the photoproduction regime (photon virtuality $Q^2 \approx 0$) by the H1 [12] and ZEUS [13] collaborations. The leading–order (LO) NRQCD calculations and the next–to–leading-order (NLO) CSM predictions are both consistent with the data. Inelastic J/ψ production in the deep inelastic scattering (DIS) regime ($Q^2 \gtrsim 1\,\mathrm{GeV}^2$) has been studied by the H1 collaboration [14]. In this case, the LO NRQCD predictions overestimate the data, whereas the LO CSM expectations

underestimate them. The shape of the differential cross sections are reasonably well reproduced by both models, except for the inelasticity distribution in the case of LO NRQCD and for the distribution of the J/ψ transverse–momentum squared in the photon–proton centre–of–mass system in the case of the LO CSM. NLO CSM predictions are not available in the DIS regime.

Models in the framework of the semi–hard or k_T–factorisation approach [15] are also available. In these models, based on non–collinear parton dynamics governed by the BFKL [16] or CCFM [17] evolution equations, effects of non–zero gluon transverse momentum are taken into account. Cross sections are then calculated as the convolution of unintegrated (transverse–momentum dependent) gluon densities and LO off–shell matrix elements. These models [18–20] succeed in describing the p_T spectra of different quarkonium states at Fermilab and J/ψ meson production at HERA, as well as the quarkonium polarisation properties measured both at Fermilab and HERA.

This paper presents a measurement of inelastic J/ψ production in DIS and comparison of the data with NRQCD and models in the k_T–factorisation approach. The reaction $e\, p \to e\, J/\psi\, X$ is studied for $Q^2 > 2\,\mathrm{GeV}^2$. The photon–gluon fusion process leading to a J/ψ in the final state is assumed to be the dominant mechanism. Other contributions arise from the production of ψ' mesons which subsequently decay to a J/ψ, and from J/ψ and ψ' production from the resolved photon process, where the exchanged photon acts as a source of partons; the latter process, however, is suppressed at high Q^2. In addition, beauty production at high Q^2 with subsequent decay of a B meson into a J/ψ also contributes to the measured cross section; this process is suppressed due to the small beauty cross section and the small B to J/ψ branching ratio.

Inelastic J/ψ production at large Q^2 has a smaller cross section than in photoproduction but presents several interesting aspects. The contribution from the CO model is expected to be more significant; both the CO and the CS predictions should be more accurate due to the higher scale in the interaction. Also, backgrounds from diffractive processes are reduced at high Q^2. The measurements presented here are in a larger kinematic range than those previously published [14]. A measurement of the hadronic final state, X, is presented for the first time.

2   Experimental set-up

The data sample used in the analysis was collected with the ZEUS detector in the years 1996–2000 and corresponds to an integrated luminosity $\mathcal{L} = 108.8 \pm 2.2\,\mathrm{pb}^{-1}$. During the 1996–97 data taking, HERA operated with positrons of energy $E_e = 27.5\,\mathrm{GeV}$ and protons of energy $E_p = 820\,\mathrm{GeV}$, corresponding to a centre-of-mass energy $\sqrt{s} = 300\,\mathrm{GeV}$ ($\mathcal{L}_{300} =$

$32.7 \pm 0.6\,\mathrm{pb}^{-1}$). In the years 1998–2000, HERA collided electrons or positrons with protons of energy $E_p = 920\,\mathrm{GeV}$, corresponding to $\sqrt{s} = 318\,\mathrm{GeV}$ ($\mathcal{L}_{318} = 76.1 \pm 1.6\,\mathrm{pb}^{-1}$). The cross sections presented here were corrected to $\sqrt{s} = 318\,\mathrm{GeV}$ using the Monte Carlo (MC) simulation described in Section 4.

A detailed description of the ZEUS detector can be found elsewhere [21, 22]. Charged particles are tracked in the central tracking detector (CTD) [23], which operates in a magnetic field of 1.43 T provided by a thin superconducting coil. The CTD consists of 72 cylindrical drift chamber layers, organised in 9 superlayers covering the polar–angle[1] region $15° < \theta < 164°$. The transverse–momentum resolution for full–length tracks is $\sigma(p_T)/p_T = 0.0058 p_T \oplus 0.0065 \oplus 0.0014/p_T$, with p_T in GeV. Energy deposits are measured in the high–resolution uranium–scintillator calorimeter (CAL) [24] which consists of three parts: the forward (FCAL), the barrel (BCAL) and the rear (RCAL) calorimeters. Each part is subdivided transversely into towers and longitudinally into one electromagnetic section (EMC) and either one (in RCAL) or two (in BCAL and FCAL) hadronic sections (HAC). The smallest subdivision of the calorimeter is called a cell. The CAL energy resolutions, as measured under test-beam conditions, are $\sigma(E)/E = 0.18/\sqrt{E}$ for electrons and $\sigma(E)/E = 0.35/\sqrt{E}$ for hadrons with E in GeV. The scattered electron[2] identification is performed by combining information from the CAL, the small–angle rear tracking detector (SRTD) [25, 26] and the hadron–electron separator (HES) [27]. Muon identification is performed by finding tracks in the barrel and rear muon chambers (BMUON and RMUON) [28] or minimum–ionising energy deposits in the CAL, matched to CTD tracks. The muon chambers are placed inside and outside a magnetised iron yoke surrounding the CAL. The barrel and rear inner muon chambers, used in this analysis, cover polar angles from 34° to 135° and from 135° to 171°, respectively.

The luminosity was determined from the rate of the electron–proton bremsstrahlung process, $ep \to e\gamma p$, where the photon was measured by a lead–scintillator calorimeter [29] located at $Z = -107$ m.

---

[1] The ZEUS coordinate system is a right-handed Cartesian system, with the Z axis pointing in the proton beam direction, referred to as the "forward direction", and the X axis pointing left towards the centre of HERA. The coordinate origin is at the nominal interaction point.

[2] Here and in the following, the term "electron" denotes generically both the electron (e^-) and the positron (e^+).

3 Event selection and reconstruction

3.1 Event selection

A three–level trigger system was used to select events online [22, 30]. The first– and second–level trigger selections were based on the identification of a scattered electron in the CAL, as described in detail elsewhere [26]. The third–level trigger selection required both a scattered electron in the CAL and a track segment reconstructed in the barrel or rear inner muon chambers.

Additional requirements were imposed in the offline selection in order to suppress the photoproduction background and select inelastic events with a J/ψ candidate identified by the presence of a pair of oppositely charged muons. In addition, the Z position of the reconstructed vertex was required to lie within $50\,\mathrm{cm}$ of the nominal interaction point.

3.2 Reconstruction of DIS kinematic variables

A scattered electron candidate, identified from the pattern of the energy deposits in the CAL [31], was required. The electron position measurement of the CAL was improved using information from the SRTD and the HES. To ensure full containment of the electromagnetic shower, the electron impact position on the inner face of the rear calorimeter was required to lie outside the box $|X| < 13\,\mathrm{cm}$, $|Y| < 7\,\mathrm{cm}$. The energy of the scattered electron was required to be greater than $10\,\mathrm{GeV}$.

The photon virtuality, Q^2, was reconstructed from the polar angle and energy of the scattered electron and was required to be in the range $2 < Q^2 < 80\,\mathrm{GeV}^2$. The Bjorken variable, $y = (P \cdot q)/(P \cdot k)$, where P, q and k are the four–momenta of the incoming proton, exchanged photon and incoming electron, respectively, was reconstructed with the Σ method [32]. Monte Carlo studies showed this method to be the most precise in the selected phase space region. The photon–proton centre–of–mass energy, W, calculated from $W^2 = ys - Q^2$, was restricted to the range $50 < W < 250\,\mathrm{GeV}$.

Conservation of energy, E, and longitudinal momentum, p_Z, require $\delta = \Sigma_i \left(E_i - p_{Z,i} \right) = 2E_e = 55\,\mathrm{GeV}$, where the sum runs over all the particles in the final state. The experimentally reconstructed quantity $\delta_{\mathrm{meas}} = \Sigma_i \left(E_i - p_{Z,i} \right)$ was calculated, where the sum runs over all final–state energy–flow objects [33] (EFOs) which combine the information from calorimetry and tracking. Only events with $40 < \delta_{\mathrm{meas}} < 65\,\mathrm{GeV}$ were kept. This cut reduces background from photoproduction events, where the scattered electron is not detected, and removes DIS events with large initial–state radiation, where the incoming electron radiates a high–energy photon before the interaction and the photon escapes

detection in the rear beam hole. To reduce background from photoproduction events further, the condition $y_e < 0.95$ was applied, where y_e indicates the value of y reconstructed from the scattered electron energy and polar angle. In order to ensure an accurate reconstruction of the final state, it was also required that the value of y, obtained with the Jacquet–Blondel method [34], be larger than 0.02.

3.3 J/ψ reconstruction

The oppositely charged muons from the J/ψ decays were reconstructed in the CTD. Each track considered in the analysis was required to be fitted to the event vertex, to reach at least the third superlayer of the CTD and to have transverse momentum $p_T > 100\,\mathrm{MeV}$; this guarantees good reconstruction quality. At least one of the tracks from the J/ψ decay had to match a segment in the inner muon chambers and the other had to match a CAL cluster with an energy deposit consistent with the passage of a minimum ionising particle (mip). To ensure high muon–identification efficiency and purity, the track matched with the segment in the barrel (rear) inner muon chambers was required to have $p_T > 1.4\,\mathrm{GeV}$ ($p > 1.8\,\mathrm{GeV}$, where p is the track momentum). For the track matched to the mip cluster in the CAL, the cut $p > 1\,\mathrm{GeV}$ was applied. The muon identification and reconstruction efficiencies were estimated separately for muons reconstructed in the BMUON, RMUON and CAL using independent samples of dimuon events. The efficiency for tracks matched to the inner muon chambers varies from 35% for $p_T \sim 1.4\,\mathrm{GeV}$ to 60% at high transverse momentum for the barrel inner muon chambers and from 50% for $p \sim 1.8\,\mathrm{GeV}$ to 65% at high momentum for the rear inner muon chambers. The efficiency for tracks matched to a mip in the CAL was 92%.

The J/ψ rapidity in the laboratory frame, defined as $Y_{\mathrm{lab}} = \frac{1}{2}\ln[(E_\psi + p_{Z,\psi})/(E_\psi - p_{Z,\psi})]$, where E_ψ and $p_{Z,\psi}$ are the energy and longitudinal momentum of the J/ψ meson, was limited to the region $-1.6 < Y_{\mathrm{lab}} < 1.3$, where the acceptance is high.

The inelasticity of the J/ψ meson, $z = (P \cdot p_\psi)/(P \cdot q)$, where p_ψ is the four–momentum of the J/ψ, was reconstructed using the expression

$$z = \frac{E_\psi - p_{Z,\psi}}{2\,E_e\,y_\Sigma},$$

where $y_\Sigma = \sum_i^{\mathrm{had}}(E_i - p_{Z,i})/\delta_{\mathrm{meas}}$ and the sum in the numerator runs over all EFOs not associated with the scattered electron. According to MC studies, the average resolution in z is 10%. The inelasticity was restricted to the range $0.2 < z < 0.9$. The lower z cut removes the region of high non-resonant background due to fake muons and the upper z cut removes elastic J/ψ events and suppresses diffractive J/ψ production with dissociation of the proton. In order to suppress further the latter background, the following cuts were applied:

- the analysis was restricted to events with an energy deposit greater than $1\,\mathrm{GeV}$ in a cone of $35°$ along the outgoing proton beam direction (excluding calorimeter deposits due to the decay muons);

- the event was required to have at least one track in addition to those associated with the two muons and with the scattered electron.

Figure 1 shows the invariant mass, $M_{\mu^+\mu^-}$, distribution of all selected muon pairs. The distribution was fitted in the intervals $2.5 < M_{\mu^+\mu^-} < 3.6\,\mathrm{GeV}$ and $3.8 < M_{\mu^+\mu^-} < 4.5\,\mathrm{GeV}$ with a function taken to be the sum of a "modified" Gaussian, to describe the signal, and a linear function, to describe the non-resonant background. The range $3.6 < M_{\mu^+\mu^-} < 3.8\,\mathrm{GeV}$ was excluded to avoid any overestimation of the background due to the ψ' state. The modified Gaussian function had the form:

$$\mathrm{Gauss}^{\mathrm{mod}} \propto \exp[-0.5 \cdot x^{1+1/(1+0.5\cdot x)}],$$

where $x = |(M_{\mu^+\mu^-} - M_0)/\sigma|$. This function was introduced to take into account the non–Gaussian tails of the resonant signal. This functional form describes both data and MC signals well. The position of the Gaussian, M_0, the signal width, σ, as well as the number of signal events were free parameters of the fit. The fit yielded a peak position of $M_0 = 3098 \pm 3$ MeV, in agreement with the PDG value [35], and a width of $\sigma = 35 \pm 3$ MeV, in agreement with the MC estimation of the detector resolution. The number of J/ψ mesons was 338 ± 25.

4   Monte Carlo models

Inelastic J/ψ events were generated using the Epjpsi [36] MC generator. Epjpsi incorporates the photon–gluon fusion process at LO, with initial– and final–state parton showers performed according to the colour–dipole model as implemented in Ariadne [37]. J/ψ mesons were produced in the framework of the CSM. The GRV98 [38] parton distribution functions were used. The scales for the evaluation of the strong coupling constant and the proton structure function were set to the centre–of–mass energy in the $\gamma^* g$ frame. The hadronisation was performed with the Lund string model [39]. The Epjpsi MC predictions were reweighted to the data in Q^2 and p_T^{*2}, where p_T^{*2} is J/ψ transverse momentum squared in the γp centre–of–mass frame. The helicity parameter in the Epjpsi MC was set to zero; this hypothesis is supported by the data [13].

Signal events were also generated using the Cascade MC program [40]. Cascade incorporates the off-shell matrix elements for the photon–gluon fusion process at LO. The initial–state parton shower is generated according to the CCFM evolution equations [17].

The J/ψ mesons were produced in the framework of the CSM. The gluon density, un-integrated in transverse momentum, k_T, was obtained from an analysis of the proton structure functions based on the CCFM equations [41]; in the event generation the gluon density used corresponds to the set named "J2003 set 2". In Cascade the hadronisation was also performed with the Lund string model.

Events with diffractive dissociation of the proton, $ep \rightarrow eJ/\psi N$, where N is a low mass state with the quantum numbers of the proton, were simulated using the Epsoft MC generator [42], which has been tuned to describe such processes at HERA [43]. Proton-dissociative events were also simulated with the Diffvm [44] MC generator. Diffvm has a more detailed simulation of the final state than Epsoft.

J/ψ mesons originating from B–meson decay were simulated using the Rapgap MC generator [45], via the photon–gluon fusion process, $\gamma^* g \rightarrow b\bar{b}$; the beauty–quark mass was set to 4.75 GeV. The CTEQ5L [46] parton distribution functions were used. The B to J/ψ branching ratio in Rapgap was set to the PDG value [35]. The MC prediction was normalised to the measured beauty cross section in DIS [47].

All generated events were passed through a full simulation of the ZEUS detector based on Geant 3.13 [48]. They were then subjected to the same trigger requirements and processed by the same reconstruction programmes as for the data.

5 Cross-section calculation

Prior to the cross–section calculation, the residual diffractive proton–dissociative background was subtracted. Although such events are produced at $z \sim 1$ and the inelasticity was restricted to $0.2 < z < 0.9$, some diffractive events migrate into the data sample due to the finite z resolution. The reconstructed track multiplicity distribution was fitted to the sum of inelastic (Epjpsi) and diffractive (Epsoft) MC predictions. The fit yielded a contribution of $6 \pm 1\%$ from proton dissociation for the whole sample. The proton–dissociative contributions were subtracted bin–by–bin from all measured cross sections according to the Epsoft predictions normalised to the above fraction.

The number of J/ψ mesons reconstructed in the kinematic region $2 < Q^2 < 80\,\text{GeV}^2$, $50 < W < 250\,\text{GeV}$, $0.2 < z < 0.9$ and $-1.6 < Y_{\text{lab}} < 1.3$, after subtraction of the proton–dissociative admixture, was compared to the predictions of the Epjpsi MC generator. The results are shown in Fig. 2 for z, Q^2, W, p_T^{*2}, the J/ψ rapidity in the γp frame[3], Y^*, and M_X^2, where M_X is the invariant mass of the final state excluding the J/ψ and the scattered electron.

---

[3] In the γp centre–of–mass frame, the photon direction was chosen to be the "forward direction".

Data were corrected bin–by–bin for geometric acceptance, detector, trigger and reconstruction inefficiencies, as well as for detector resolution, using the EPJPSI MC generator. The acceptance, $A_i(\mathcal{O})$, as a function of an observable, $\mathcal{O}$, in a given bin, i, is $A_i(\mathcal{O}) = N_i^{\text{rec}}(\mathcal{O})/N_i^{\text{gen}}(\mathcal{O})$, where $N_i^{\text{gen}}(\mathcal{O})$ is the number of generated MC events and $N_i^{\text{rec}}(\mathcal{O})$ is the number of reconstructed events passing all the selection requirements.

Differential cross sections as a function of $\mathcal{O}$ in a given bin i were obtained using the expression

$$\frac{d\sigma_i}{d\mathcal{O}} = \frac{N_i}{\mathcal{B} \ \mathcal{L} \ A_i(\mathcal{O})},$$

where N_i is the number of signal events, reconstructed in each bin after subtraction of the estimated contribution from the diffractive proton–dissociative events, $\mathcal{B}$ the branching ratio $(5.88 \pm 0.10)\%$ [35] and $\mathcal{L}$ the integrated luminosity.

The background from ψ' photoproduction is expected to be 15% [49]; this expectation was confirmed by a direct measurement of the ψ' to J/ψ cross section ratio [13]. Restricting the phase–space region in this analysis similar to that for photoproduction, $50 < W < 180\,\text{GeV}$ and $0.55 < z < 0.9$, the number of observed ψ' events was consistent with the expectation from the ψ' to J/ψ ratio measured in the photoproduction regime. The contribution of J/ψ mesons from ψ' decays was assumed to yield the same kinematic distributions as the dominant direct J/ψ contribution and, therefore, the theoretical predictions for J/ψ production were scaled up by 15%. This change is small compared to the normalisation error of the LO NRQCD predictions.

Monte Carlo studies showed that the contribution from B–meson decays into J/ψ was concentrated at low–z values and small elsewhere. For $0.1 < z < 0.4$, this contribution can be as large as 20%. The beauty contribution was estimated using the RAPGAP MC and added to the J/ψ predictions. This change is small compared to the normalisation uncertainty of the LO NRQCD predictions.

The J/ψ meson can be produced via χ_c radiative decays, $\chi_c \to J/\psi\gamma$. While χ_c mesons can be produced copiously in hadron–hadron collisions through gg, gq and $q\bar{q}$ interactions, χ_c production via photon–gluon fusion is forbidden at LO in the CS model. This leaves only resolved photon processes, strongly suppressed at non–zero photon virtuality, or CO processes as sources of χ_c production. However, the ratio of the χ_c to J/ψ from the CO processes is expected to be below 1% [50]. This contribution was therefore neglected.

The effect of the LO electroweak corrections was studied using the HERACLES [51] MC program. The open charm DIS cross section was evaluated using the RAPGAP [45] MC program with and without radiative corrections, as calculated by HERACLES, in a W–Q^2 grid. The measured cross sections were then corrected to the QED Born level using the HERACLES predictions. In the region covered by the data, this correction was -2% on average and always below 7% in absolute value.

6 Systematic uncertainties

The systematic uncertainties of the measured differential cross sections were determined by changing the selection cuts or the analysis procedure in turn and repeating the extraction of the differential cross sections. The resulting uncertainty on the total cross section is given in parentheses. The following categories of systematic uncertainties were considered:

- scattered electron reconstruction: these uncertainties were evaluated as described elsewhere [52] (2%);

- CAL energy scale and resolution simulation: these uncertainties were evaluated as described elsewhere [52] (2%);

- tracking: the resolutions on track momenta and angles were varied by $\pm$ 20% of their values and the magnetic field by $\pm$ 0.3% (1%);

- muon reconstruction: the uncertainty of the muon acceptance, including those of the efficiency of the muon chambers, the trigger selection algorithms and the offline reconstruction, was obtained from a study based on an independent dimuon sample at high Q^2, performed following the method discussed elsewhere [53] (6%);

- fitting procedure: the invariant–mass range and the functional form of the background were varied (2%);

- simulation of the process $\gamma^* g \to J/\psi g$: the CASCADE MC rather than the EPJPSI MC was used to calculate acceptances (5%);

- subtraction of the remaining diffractive proton–dissociative admixture: DIFFVM rather than EPSOFT was used to perform the subtraction of the proton diffractive events (3%).

These estimations were also made in each bin of the differential cross sections. All of the above individual sources of systematic uncertainty were added in quadrature.

The following sources resulted in an overall shift of the cross section and were therefore treated as normalisation uncertainties:

- the integrated luminosity determination has an uncertainty of 2%;

- the branching ratio of $J/\psi \to \mu^+ \mu^-$ has an uncertainty of 1.7% [35].

The normalisation uncertainties were not included in the total systematic uncertainty.

7 Results

The cross section for the process $ep \to e J/\psi X$ in the kinematic region $2 < Q^2 < 80 \, \text{GeV}^2$, $50 < W < 250 \, \text{GeV}$, $0.2 < z < 0.9$ and $-1.6 < Y_{\text{lab}} < 1.3$ is

$$302 \pm 23 \text{ (stat.)} \; ^{+28}_{-20} \text{ (syst.) pb,}$$

where the first uncertainty is statistical and the second systematic. In Figs. 3, 4 and 5, the differential cross sections as a function of z, Q^2, W, p_T^{*2}, Y^*, $\log M_X^2$ and the rapidity of the hadronic system X, Y_X, are shown. They are compared to the predictions of a NRQCD model [54], a CS model with k_T factorisation (LZ) [18] and to the CASCADE MC. The beauty contribution, estimated using the RAPGAP MC, is also shown separately in Figs. 3c and 4a. All differential cross sections and normalised cross sections are given in Tables 1 and 2.

The uncertainties for the CS and CO NRQCD predictions correspond to variations of the charm–quark mass ($m_c = 1.5 \pm 0.1\,\text{GeV}$) and of the renormalisation and factorisation scales from $\frac{1}{2}\sqrt{Q^2 + M_\psi^2}$ to $2\sqrt{Q^2 + M_\psi^2}$. The uncertainty on the long–distance matrix elements and the effect of different choices of parton distribution functions (default set is MRST98LO) are also taken into account. The bands in the figures shows all these uncertainties added in quadrature.

In general, the CSM is consistent with the data. The predictions including both CS and CO contributions are higher than the data, especially at high z and low p_T^{*2}. At high values of p_T^{*2} the agreement with the data is reasonable. The prediction does not describe the shapes of the z, Y^*, $\log M_X^2$ and Y_X distributions. Previous photoproduction results [12, 13] showed that the agreement between data and theory at high z can be improved using resummed LO NRQCD predictions [55]. It should be noted that, in photoproduction, inclusion of the NLO corrections to the CSM, not available for DIS, significantly improved the description of the data.

For the LZ k_T–factorisation predictions, the parametrisation, KMS [56], of the unintegrated gluon density was used. The charm–quark mass was set to $m_c = 1.4\,\text{GeV}$, which is the mass used in the KMS parametrisation. The renormalisation and factorisation scales were both set to $\mu = k_T$ for $k_T > 1\,\text{GeV}$. For $k_T \leq 1$ GeV the scales were fixed at 1 GeV. Calculations based on the k_T-factorisation approach give a reasonable description of the data both in shape and normalisation.

The data are also compared with the predictions of the CASCADE MC using the k_T-factorisation approach, where gluons are treated according to the CCFM evolution equations. These predictions were obtained by setting the charm–quark mass to 1.5 GeV, the evolution scale of the strong coupling constant to the J/ψ transverse mass, $\sqrt{M_\psi^2 + p_T^2}$, and using the unintegrated gluon–density parametrisation "J2003 set 2". The CASCADE MC is above the data for $z > 0.45$ and for $W < 175\,\text{GeV}$.

In order to compare the present measurements directly to the H1 results [14], differential cross sections were determined in the kinematic range $2 < Q^2 < 100\,\text{GeV}^2$, $50 < W < 225\,\text{GeV}$, $0.3 < z < 0.9$ and $p_T^{*2} > 1\,\text{GeV}^2$; all ZEUS differential cross sections and

normalised cross sections are given in Table 3. The results of this comparison are shown in Fig. 6. The present results are in agreement with those from H1. In Fig. 3a, the ZEUS data are in better agreement with the CSM prediction than in Fig. 6a. This is a consequence of the $p_T^{*2} > 1\,\mathrm{GeV}^2$ cut used in Fig. 6a combined with the fact that the CS prediction underestimate the data at high p_T^{*2}, as seen in Fig. 4a.

8 Conclusions

Inelastic J/ψ production in DIS has been measured in the kinematic region $2 < Q^2 < 80\,\mathrm{GeV}^2$, $50 < W < 250\,\mathrm{GeV}$, $0.2 < z < 0.9$ and $-1.6 < Y_{\mathrm{lab}} < 1.3$. The data are in agreement with the H1 results in the kinematic region $2 < Q^2 < 100\,\mathrm{GeV}^2$, $50 < W < 225\,\mathrm{GeV}$, $0.3 < z < 0.9$ and $p_T^{*2} > 1\,\mathrm{GeV}^2$. The data are compared with LO NRQCD predictions, including both CS and CO contributions, and k_T–factorisation calculations. Calculations of the CS process generally agree with the data, whereas inclusion of CO terms spoils this agreement.

Acknowledgments

References

[1] NMC Coll., D. Allasia et al., Phys. Lett. **B 258**, 493 (1991);
EMC Coll., J. J. Aubert et al., Nucl. Phys. **B 213**, 1 (1983);
UA1 Coll., C. Albajar et al., Phys. Lett. **B 256**, 112 (1991).

[2] CDF Coll., F. Abe et al., Phys. Rev. Lett. **69**, 3704 (1992).

[3] E. L. Berger and D. Jones, Phys. Rev. **D 23**, 1521 (1981).

[4] CDF Coll., F. Abe et al., Phys. Rev. Lett. **79**, 572 (1997);
CDF Coll., F. Abe et al., Phys. Rev. Lett. **79**, 578 (1997).

[5] G. T. Bodwin, E. Braaten and G. P. Lepage, Phys. Rev. **D 51**, 1125 (1995).
Erratum-ibid **D 55**, 5853 (1997).

[6] DELPHI Coll., J. Abdallah et al., Phys. Lett. **B 565**, 76 (2003).

[7] CDF Coll., T. Affolder et al., Phys. Rev. Lett. **85**, 2886 (2000).

[8] BaBar Coll., B. Aubert et al., Phys. Rev. Lett. **87**, 162002 (2001).

[9] Belle Coll., K. Abe et al., Phys. Rev. Lett. **88**, 52001 (2002).

[10] H1 Coll., C. Adloff et al., Phys. Lett. **B 483**, 23 (2000);
H1 Coll., A. Aktas et al., Phys. Lett. **B 568**, 205 (2003).

[11] ZEUS Coll., S. Chekanov et al., Eur. Phys. J. **C 24**, 345 (2002);
ZEUS Coll., S. Chekanov et al., Eur. Phys. J. **C 26**, 389 (2003).

[12] H1 Coll., C. Adloff et al., Eur. Phys. J. **C 25**, 25 (2002).

[13] ZEUS Coll., S. Chekanov et al., Eur. Phys. J. **C 27**, 173 (2003).

[14] H1 Coll., C. Adloff et al., Eur. Phys. J. **C 25**, 41 (2002).

[15] L.V. Gribov, E.M. Levin and M.G. Ryskin, Phys. Rep. **100**, 1 (1983);
E.M. Levin and M.G. Ryskin, Phys. Rep. **189**, 267 (1990);
E.M. Levin et al., Sov. J. Nucl. Phys. **53**, 657 (1991);
E.M. Levin et al., Sov. J. Nucl. Phys. **54**, 867 (1991);
S. Catani, M. Ciafaloni and F. Hautmann, Phys. Lett. **B 242**, 97 (1990);
S. Catani, M. Ciafaloni and F. Hautmann, Nucl. Phys. **B 366**, 135 (1991);
J.C. Collins and R.K. Ellis, Nucl. Phys. **B 360**, 3 (1991);
G. Marchesini and R.K. Webber, Nucl. Phys. **B 386**, 215 (1992).

[16] E.A. Kuraev, L.N. Lipatov and V.S. Fadin, Sov. Phys. JETP **44**, 443 (1976);
E.A. Kuraev, L.N. Lipatov and V.S. Fadin, Sov. Phys. JETP **45**, 199 (1977);
Ya.Ya. Balitskiĭ and L.N. Lipatov, Sov. J. Nucl. Phys. **28**, 822 (1978).

[17] M. Ciafaloni, Nucl. Phys. **B 296**, 49 (1988);
S. Catani, F. Fiorani and G. Marchesini, Phys. Lett. **B 234**, 339 (1990).

[18] A. V. Lipatov and N. P. Zotov, Eur. Phys. J. **C 27**, 87 (2003).

[19] S. P. Baranov and N. P. Zotov, J. Phys., **G 29**, 1395 (2003).

[20] S. P. Baranov, Phys. Rev. **D 66**, 114003 (2002).

[21] ZEUS Coll., M. Derrick et al., Phys. Lett. **B 293**, 465 (1992).

[22] ZEUS Coll., U. Holm (ed.), *The ZEUS Detector*. Status Report (unpublished),
DESY (1993), available on `http://www-zeus.desy.de/bluebook/bluebook.html`.

[23] N. Harnew et al., Nucl. Inst. Meth. **A 279**, 290 (1989);
B. Foster et al., Nucl. Phys. Proc. Suppl. **B 32**, 181 (1993);
B. Foster et al., Nucl. Inst. Meth. **A 338**, 254 (1994).

[24] M. Derrick et al., Nucl. Inst. Meth. **A 309**, 77 (1991);
A. Andresen et al., Nucl. Inst. Meth. **A 309**, 101 (1991);
A. Caldwell et al., Nucl. Inst. Meth. **A 321**, 356 (1992);
A. Bernstein et al., Nucl. Inst. Meth. **A 336**, 23 (1993).

[25] A. Bamberger et al., Nucl. Inst. Meth. **A 401**, 63 (1997).

[26] ZEUS Coll., S. Chekanov et al., Eur. Phys. J. **C 21**, 443 (2001).

[27] A. Dwurazny et al., Nucl. Inst. Meth. **A 277**, 176 (1989).

[28] G. Abbiendi et al., Nucl. Inst. Meth. **A 333**, 342 (1993).

[29] J. Andruszków et al., Preprint DESY-92-066, DESY, 1992;
ZEUS Coll., M. Derrick et al., Z. Phys. **C 63**, 391 (1994);
J. Andruszków et al., Acta Phys. Pol. **B 32**, 2025 (2001).

[30] W. H. Smith, K. Tokushuku and L. W. Wiggers, *Proc. Computing in High-Energy Physics (CHEP), Annecy, France, Sept. 1992*, C. Verkerk and W. Wojcik (eds.), p. 222. CERN, Geneva, Switzerland (1992). Also in preprint DESY 92-150B.

[31] H. Abramowicz, A. Caldwell and R. Sinkus, Nucl. Inst. Meth. **A 365**, 508 (1995);
R. Sinkus and T. Voss, Nucl. Inst. Meth. **A 391**, 360 (1997).

[32] U. Bassler and G. Bernardi, Nucl. Inst. Meth. **A 361**, 197 (1995).

[33] ZEUS Coll., J. Breitweg et al., Eur. Phys. J. **C 1**, 81 (1998);
G. M. Briskin, Ph.D. Thesis, Tel Aviv University, (1998). DESY-THESIS-1999-036.

[34] F. Jacquet and A. Blondel, *Proc. the Study of an eP Facility for Europe*,
U. Amaldi (ed.), p. 391. (1979). Also in preprint DESY 79-48.

[35] Particle Data Group, S. Eidelman et al., Phys. Lett. **B 592**, 1 (2004).

[36] H. Jung, *Proc. Workshop on Physics at HERA*, W. Buchmüller and
G. Ingelman (eds.), Vol. 3, p. 1488, DESY, Hamburg, Germany (1992);
H. Jung et al., Z. Phys. **C 60**, 721 (1993).

[37] L. Lönnblad, Comp. Phys. Comm. **71**, 15 (1992).

[38] M. Glück, E. Reya and A. Vogt, Eur. Phys. J. **C 5**, 461 (1998).

[39] B. Andersson et al., Phys. Rep. **97**, 31 (1983).

[40] H. Jung and G. P. Salam, Eur. Phys. J. **C 19** (2001).

[41] H. Jung, Mod. Phys. Lett., **A 19**, 1 (2004).

[42] M. Kasprzak, Ph.D. Thesis, Warsaw University, Warsaw, Poland (1996).
DESY F35D-96-16.

[43] L. Adamczyk, Ph.D. Thesis, University of Mining and Metallurgy, Cracow, Poland
(1999). DESY-THESIS-1999-045.

[44] B. List and A. Mastroberardino, *Proc. Workshop on Monte Carlo Generators for
HERA Physics*, A.T. Doyle, et al. (eds.), p. 396. DESY, Hamburg, Germany
(1999). Also in preprint DESY-PROC-1999-02, available on
`http://www.desy.de/~heramc/.`

[45] H. Jung, Comp. Phys. Comm. **86**, 147 (1995).

[46] CTEQ Coll., H.L. Lai et al., Eur. Phys. J. **C 12**, 375 (2000).

[47] ZEUS Coll., S. Chekanov et al., Phys. Lett. **B 599**, 173 (2004).

[48] R. Brun et al., GEANT3, Technical Report CERN-DD/EE/84-1, CERN, 1987.

[49] M. Krämer et al., Phys. Lett. **B 348**, 657 (1995);
M. Krämer, Nucl. Phys. **B 459**, 3 (1996).

[50] M. Krämer, Prog. Part. Nucl. Phys., **47**, 141 (2001).

[51] A. Kwiatkowski, H. Spiesberger and H.-J. Möhring, Comp. Phys. Comm.
69, 155 (1992). Also in *Proc. Workshop Physics at HERA*, DESY, Hamburg (1991).

[52] ZEUS Coll., S. Chekanov et al., Phys. Rev. **D 69**, 12004 (2004).

[53] M. Turcato, Ph.D. Thesis, Padova University (2002). DESY-THESIS-2003-039.

[54] B. A. Kniehl and L. Zwirner, Nucl. Phys. **B 621**, 337 (2002).

[55] M. Beneke, G. A. Schuler and S. Wolf, Phys. Rev. **D 62**, 34004 (2000).

[56] J. Kwiecinski, A. D. Martin and A. M. Stasto, Phys. Rev. **D 56**, 3991 (1997).

z range	$d\sigma/dz$ (pb)	$1/\sigma d\sigma/dz$
$0.20 - 0.45$	$309 \pm 61^{+41}_{-34}$	$1.01 \pm 0.16^{+0.09}_{-0.08}$
$0.45 - 0.60$	$428 \pm 62^{+44}_{-32}$	$1.40 \pm 0.19^{+0.09}_{-0.06}$
$0.60 - 0.75$	$568 \pm 65^{+64}_{-55}$	$1.86 \pm 0.20^{+0.08}_{-0.13}$
$0.75 - 0.90$	$526 \pm 66^{+74}_{-47}$	$1.72 \pm 0.20^{+0.17}_{-0.15}$
W range (GeV)	$d\sigma/dW$ (pb/GeV)	$1/\sigma d\sigma/dW$
$50 - 100$	$1.73 \pm 0.25^{+0.20}_{-0.16}$	$0.0056 \pm 0.0007^{+0.0005}_{-0.0005}$
$100 - 125$	$2.44 \pm 0.32^{+0.23}_{-0.20}$	$0.0080 \pm 0.0010^{+0.0004}_{-0.0005}$
$125 - 175$	$1.43 \pm 0.20^{+0.14}_{-0.12}$	$0.0047 \pm 0.0006^{+0.0003}_{-0.0003}$
$175 - 250$	$1.17 \pm 0.22^{+0.19}_{-0.17}$	$0.0038 \pm 0.0006^{+0.0004}_{-0.0004}$
Q^2 range (GeV^2)	$d\sigma/dQ^2$ (pb/GeV^2)	$1/\sigma d\sigma/dQ^2$
$2 - 4$	$66.9 \pm 8.4^{+7.7}_{-6.8}$	$0.223 \pm 0.019^{+0.008}_{-0.012}$
$4 - 8$	$18.3 \pm 2.7^{+1.6}_{-1.3}$	$0.0609 \pm 0.0079^{+0.0033}_{-0.0028}$
$8 - 16$	$6.3 \pm 1.0^{+0.7}_{-0.6}$	$0.0211 \pm 0.0032^{+0.0013}_{-0.0015}$
$16 - 80$	$0.66 \pm 0.12^{+0.09}_{-0.05}$	$0.00221 \pm 0.00038^{+0.00026}_{-0.00014}$
p_T^{*2} range (GeV^2)	$d\sigma/dp_T^{*2}$ (pb/GeV^2)	$1/\sigma d\sigma/dp_T^{*2}$
$0 - 1$	$80 \pm 14^{+8}_{-9}$	$0.269 \pm 0.041^{+0.012}_{-0.034}$
$1 - 5$	$40.1 \pm 4.1^{+5.7}_{-2.6}$	$0.1345 \pm 0.0096^{+0.0080}_{-0.0014}$
$5 - 16$	$3.81 \pm 0.70^{+0.44}_{-0.32}$	$0.0128 \pm 0.0022^{+0.0010}_{-0.0008}$
$16 - 100$	$0.280 \pm 0.051^{+0.031}_{-0.027}$	$0.00094 \pm 0.00017^{+0.00006}_{-0.00009}$
Y^* range	$d\sigma/dY^*$ (pb)	$1/\sigma d\sigma/dY^*$
$1.75 - 2.60$	$80 \pm 16^{+9}_{-7}$	$0.274 \pm 0.045^{+0.017}_{-0.021}$
$2.60 - 3.00$	$212 \pm 28^{+30}_{-16}$	$0.722 \pm 0.083^{+0.052}_{-0.031}$
$3.00 - 3.40$	$211 \pm 25^{+18}_{-16}$	$0.716 \pm 0.077^{+0.026}_{-0.055}$
$3.40 - 4.00$	$94 \pm 14^{+18}_{-9}$	$0.321 \pm 0.045^{+0.041}_{-0.024}$

Table 1: *Differential cross sections and normalised differential cross sections in the kinematic region $2 < Q^2 < 80\,GeV^2$, $50 < W < 250\,GeV$, $0.2 < z < 0.9$ and $-1.6 < Y_{lab} < 1.3$ as a function of z, W, Q^2, p_T^{*2} and Y^*. The first uncertainty is statistical and the second is systematic. Overall normalisation uncertainties due to the luminosity measurement ($\pm 2\%$) and to the J/ψ decay branching ratio (1.7%) are not included in the systematic error.*

$\log(M_X^2/\mathrm{GeV}^2)$ range	$d\sigma/d\log(M_X^2/\mathrm{GeV}^2)$ (pb)	$1/\sigma\, d\sigma/d\log(M_X^2/\mathrm{GeV}^2)$
$3.00 - 3.55$	$156 \pm 18^{+19}_{-20}$	$0.556 \pm 0.057^{+0.052}_{-0.074}$
$3.55 - 3.85$	$208 \pm 27^{+25}_{-16}$	$0.740 \pm 0.091^{+0.056}_{-0.021}$
$3.85 - 4.10$	$270 \pm 40^{+38}_{-31}$	$0.96 \pm 0.13^{+0.09}_{-0.08}$
$4.10 - 4.50$	$164 \pm 31^{+21}_{-18}$	$0.581 \pm 0.092^{+0.054}_{-0.050}$
Y_X range	$d\sigma/dY_X$ (pb)	$1/\sigma\, d\sigma/dY_X$
$2.20 - 2.78$	$112 \pm 21^{+13}_{-11}$	$0.383 \pm 0.061^{+0.033}_{-0.033}$
$2.78 - 3.05$	$243 \pm 37^{+33}_{-26}$	$0.83 \pm 0.11^{+0.08}_{-0.07}$
$3.05 - 3.37$	$203 \pm 26^{+29}_{-15}$	$0.692 \pm 0.083^{+0.067}_{-0.018}$
$3.37 - 4.05$	$143 \pm 16^{+17}_{-18}$	$0.488 \pm 0.047^{+0.044}_{-0.063}$

Table 2: *Differential cross sections and normalised differential cross sections in the kinematic region $2 < Q^2 < 80\ GeV^2$, $50 < W < 250\ GeV$, $0.2 < z < 0.9$ and $-1.6 < Y_{lab} < 1.3$ as a function of $\log(M_X^2/GeV^2)$ and Y_X. The first uncertainty is statistical and the second is systematic. Overall normalisation uncertainties due to the luminosity measurement ($\pm 2\%$) and to the J/ψ decay branching ratio (1.7%) are not included in the systematic error.*

z range	$d\sigma/dz$ (pb)	$1/\sigma d\sigma/dz$
$0.30 - 0.45$	$246 \pm 60^{+28}_{-29}$	$1.18 \pm 0.25^{+0.07}_{-0.13}$
$0.45 - 0.60$	$317 \pm 50^{+39}_{-24}$	$1.53 \pm 0.22^{+0.13}_{-0.10}$
$0.60 - 0.75$	$430 \pm 56^{+51}_{-34}$	$2.07 \pm 0.23^{+0.09}_{-0.11}$
$0.75 - 0.90$	$392 \pm 57^{+64}_{-41}$	$1.89 \pm 0.24^{+0.22}_{-0.17}$
p^{*2}_T range (GeV^2)	$d\sigma/dp^{*2}_T$ (pb/GeV^2)	$1/\sigma d\sigma/dp^{*2}_T$
$1 - 5$	$36.4 \pm 3.7^{+4.1}_{-2.4}$	$0.1752 \pm 0.0092^{+0.0054}_{-0.0054}$
$5 - 16$	$3.65 \pm 0.71^{+0.17}_{-0.32}$	$0.0176 \pm 0.0030^{+0.0022}_{-0.0011}$
$16 - 40$	$0.92 \pm 0.18^{+0.12}_{-0.10}$	$0.00443 \pm 0.00083^{+0.00028}_{-0.00051}$
Y^* range	$d\sigma/dY^*$ (pb)	$1/\sigma d\sigma/dY^*$
$2.00 - 2.60$	$66 \pm 14^{+7}_{-10}$	$0.351 \pm 0.066^{+0.023}_{-0.048}$
$2.60 - 3.00$	$137 \pm 20^{+15}_{-10}$	$0.728 \pm 0.094^{+0.053}_{-0.048}$
$3.00 - 3.40$	$144 \pm 19^{+13}_{-11}$	$0.762 \pm 0.091^{+0.035}_{-0.049}$
$3.40 - 4.00$	$61 \pm 14^{+12}_{-6}$	$0.323 \pm 0.064^{+0.049}_{-0.025}$

Table 3: *Differential cross sections and normalised differential cross sections in the kinematic region $2 < Q^2 < 100\ GeV^2$, $50 < W < 225\ GeV$, $0.3 < z < 0.9$ and $p^{*2}_T > 1\ GeV^2$ as a function of z, p^{*2}_T and Y^*. The first uncertainty is statistical and the second is systematic. Overall normalisation uncertainties due to the luminosity measurement ($\pm 2\%$) and to the J/ψ decay branching ratio (1.7%) are not included in the systematic error.*
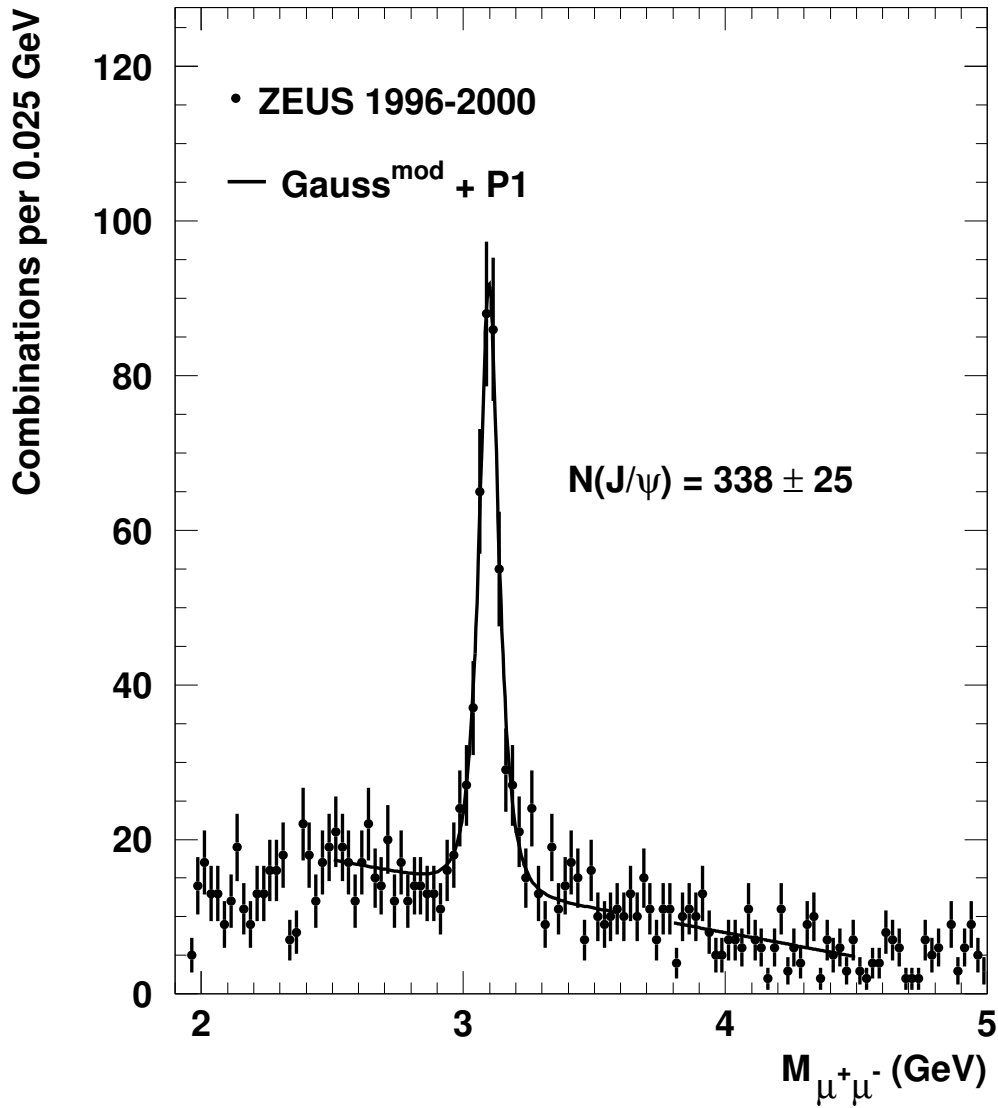
Figure 1: *Invariant mass spectrum after all selection cuts in the kinematic region $2 < Q^2 < 80\,GeV^2$, $50 < W < 250\,GeV$, $0.2 < z < 0.9$ and $-1.6 < Y_{lab} < 1.3$. The curve is the result of the fit with a modified Gaussian for the signal (see text) and a linear function (P1) for the non–resonant background.*
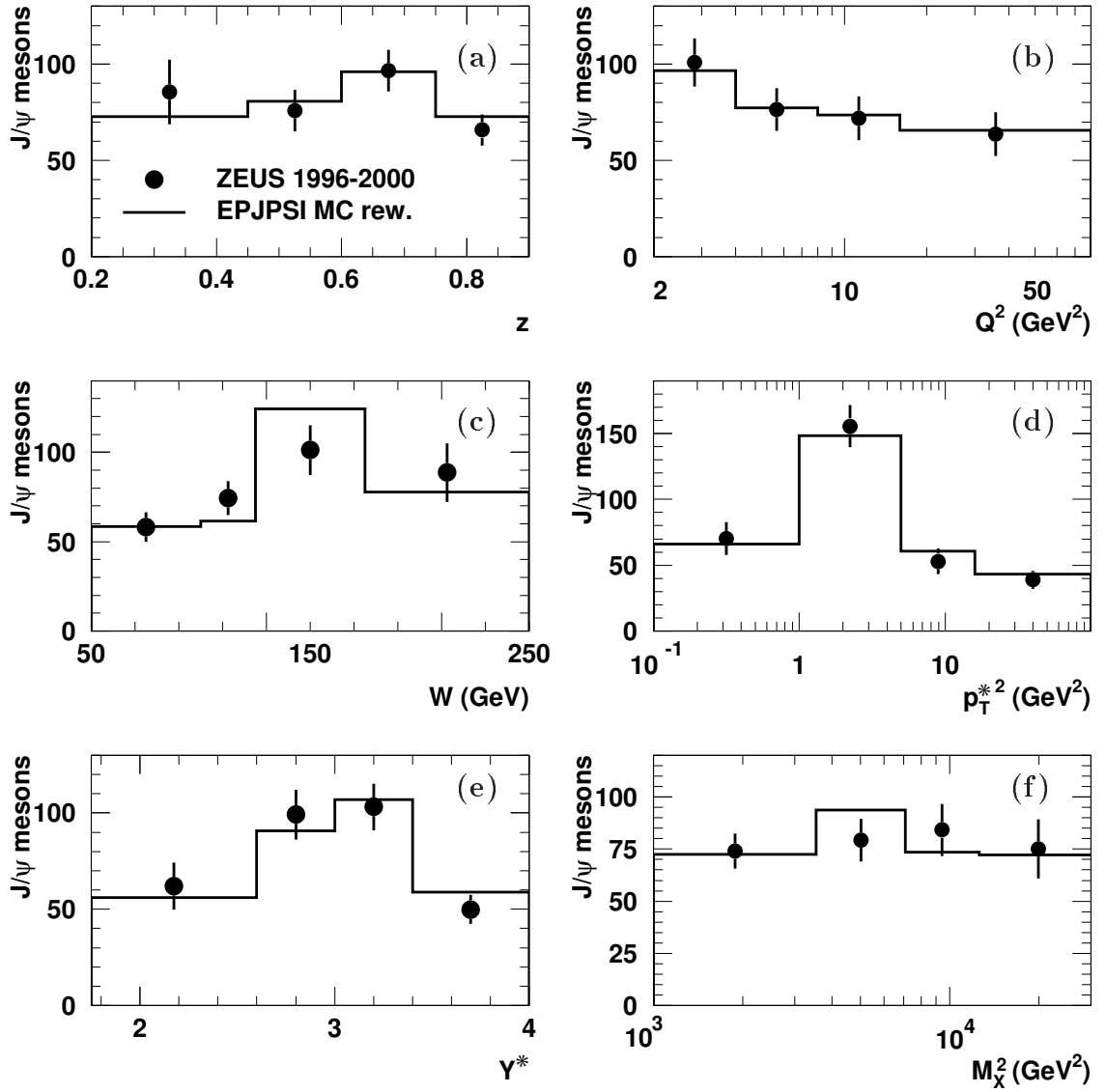
ZEUS

Figure 2: *Number of J/ψ mesons reconstructed in the kinematic region $2 < Q^2 < 80\,GeV^2$, $50 < W < 250\,GeV$, $0.2 < z < 0.9$ and $-1.6 < Y_{lab} < 1.3$ plotted as a function of (a) z, (b) Q^2, (c) W, (d) p_T^{*2}, (e) Y^* and (f) M_X^2. The data distributions are shown as the points with statistical errors only. The histograms show the EPJPSI MC predictions reweighted to the data shapes in Q^2 and p_T^{*2} and area normalised to the data.*
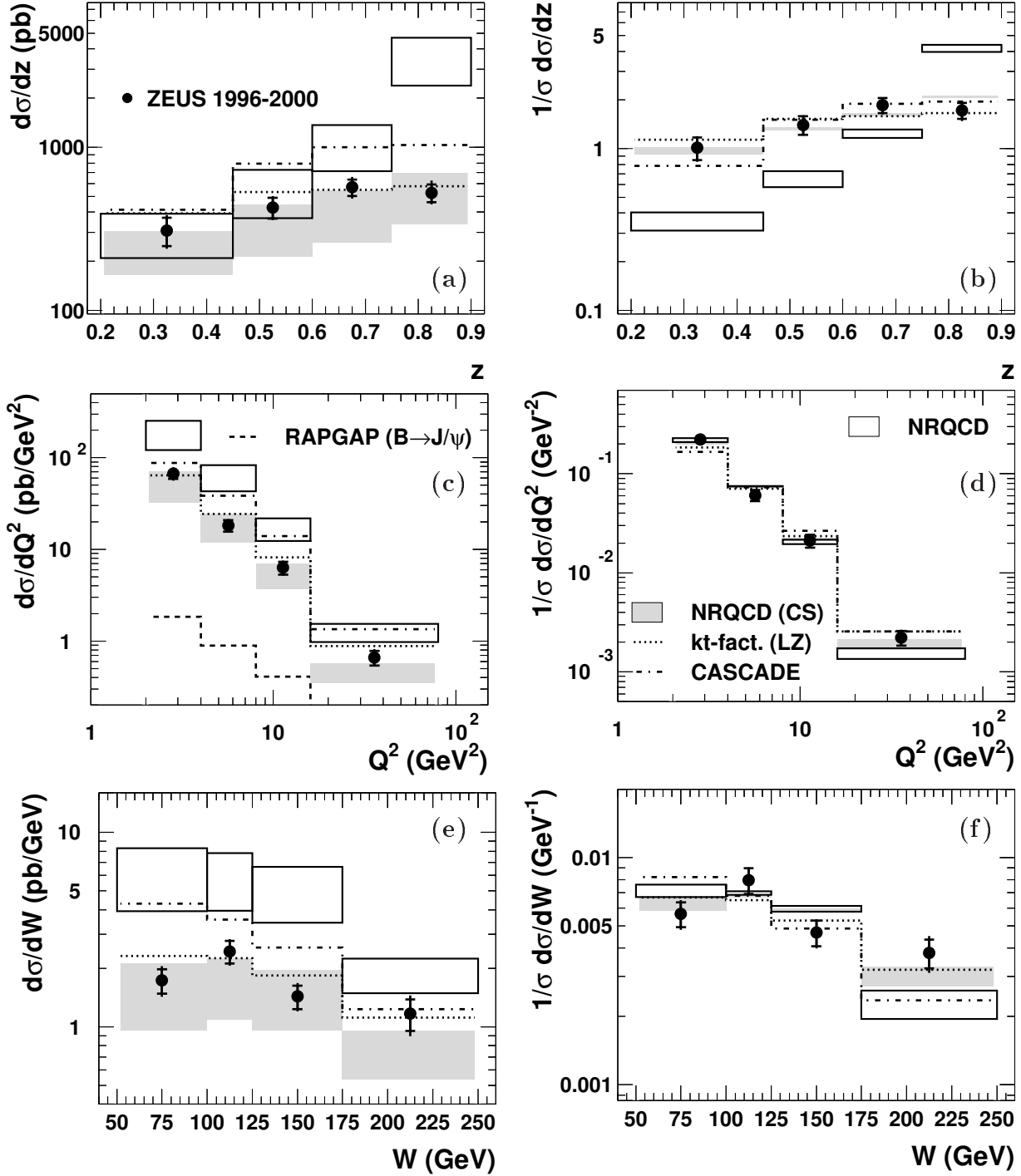
ZEUS

Figure 3: *Differential cross sections for the reaction $e\,p \rightarrow e\,J/\psi\,X$ in the kinematic region $2 < Q^2 < 80\,GeV^2$, $50 < W < 250\,GeV$, $0.2 < z < 0.9$ and $-1.6 < Y_{lab} < 1.3$ as a function of (a) z, (c) Q^2 and (e) W. The inner error bars of the data points show the statistical uncertainty; the outer bars show statistical and systematic uncertainties added in quadrature. The data are compared to LO NRQCD predictions, a LO CS calculation, a prediction in the k_T-factorisation approach within the CSM and the CASCADE MC predictions. (b), (d) and (f) show the data and the theoretical predictions normalised to unit area.*
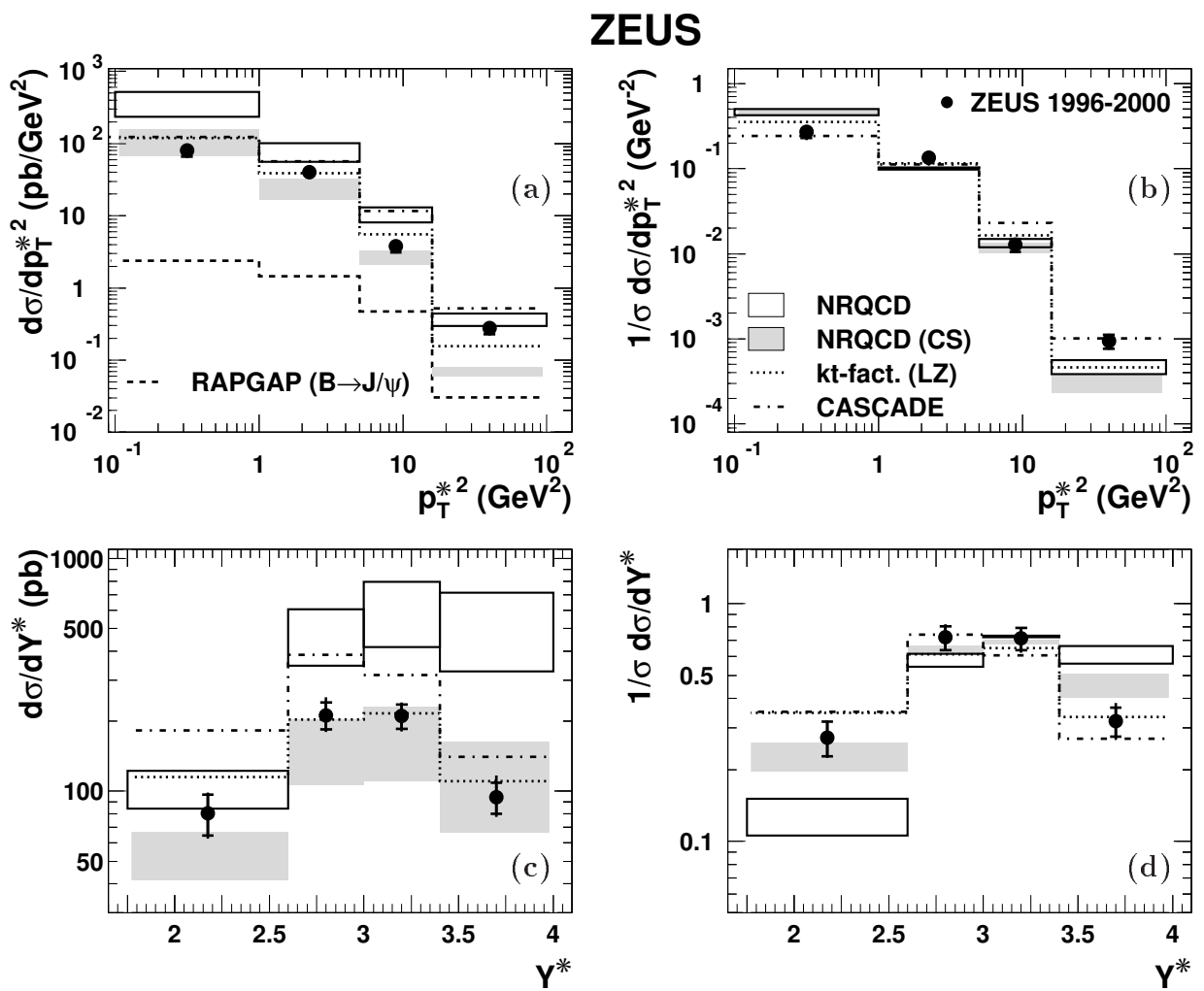
Figure 4: *Differential cross sections for the reaction* $e\,p \rightarrow e\,J/\psi\,X$ *in the kinematic region* $2 < Q^2 < 80\,GeV^2$, $50 < W < 250\,GeV$, $0.2 < z < 0.9$ *and* $-1.6 < Y_{lab} < 1.3$ *as a function of (a)* p_T^{*2} *and (c)* Y^*. *The inner error bars of the data points show the statistical uncertainty; the outer bars show statistical and systematic uncertainties added in quadrature. The data are compared to LO NRQCD predictions, a LO CS calculation, a prediction in the* k_T*–factorisation approach within the CSM and the* CASCADE *MC predictions. (b) and (d) show the data and the theoretical predictions normalised to unit area.*
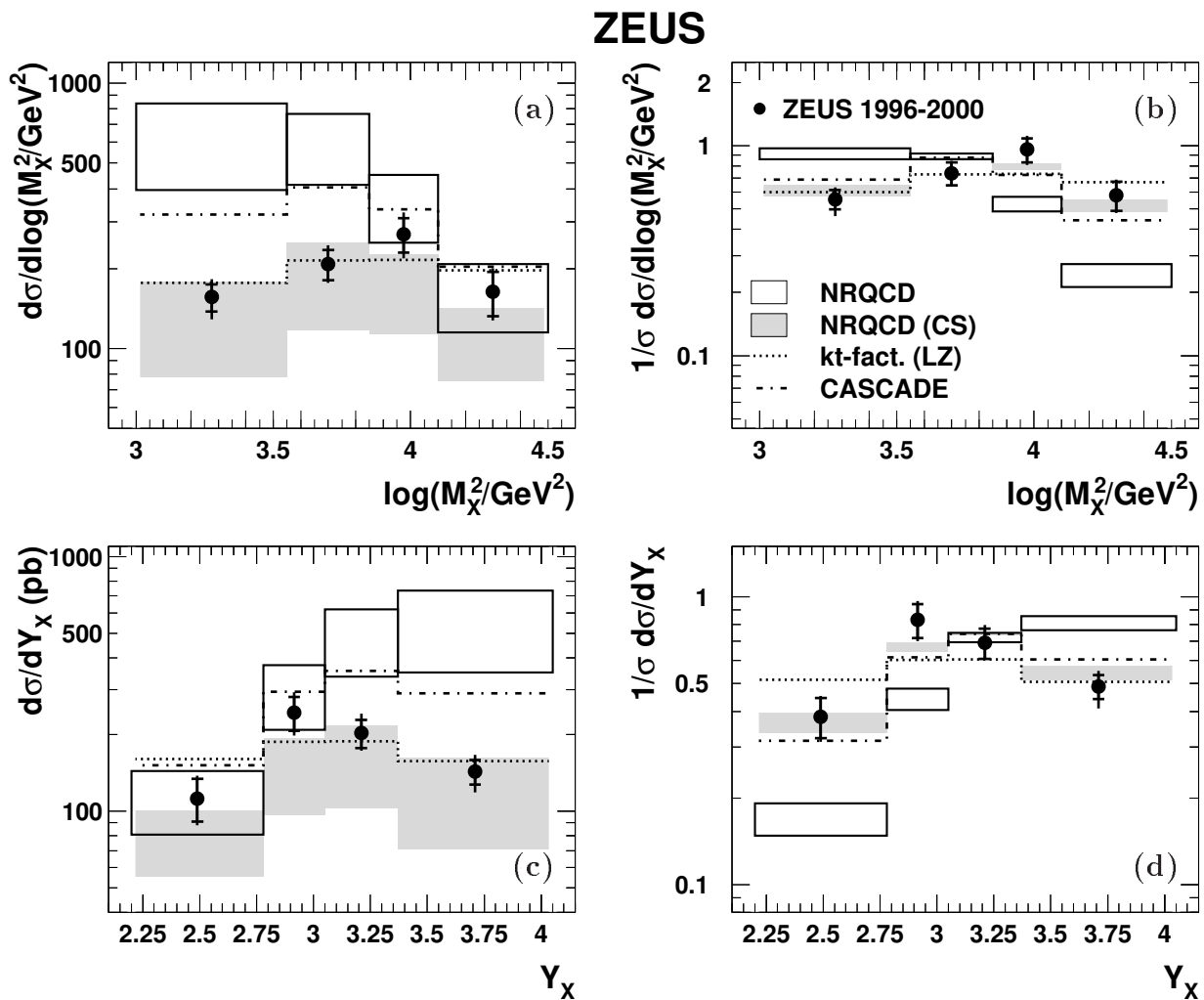
ZEUS

Figure 5: *Differential cross sections for the reaction $e\,p \to e\,J/\psi\,X$ in the kinematic region $2 < Q^2 < 80\,GeV^2$, $50 < W < 250\,GeV$, $0.2 < z < 0.9$ and $-1.6 < Y_{lab} < 1.3$ as a function of (a) $\log M_X^2$ and (c) Y_X. The inner error bars of the data points show the statistical uncertainty; the outer bars show statistical and systematic uncertainties added in quadrature. The data are compared to LO NRQCD predictions, a LO CS calculation, a prediction in the k_T–factorisation approach within the CSM and the CASCADE MC predictions. (b) and (d) show the data and the theoretical predictions normalised to unit area.*
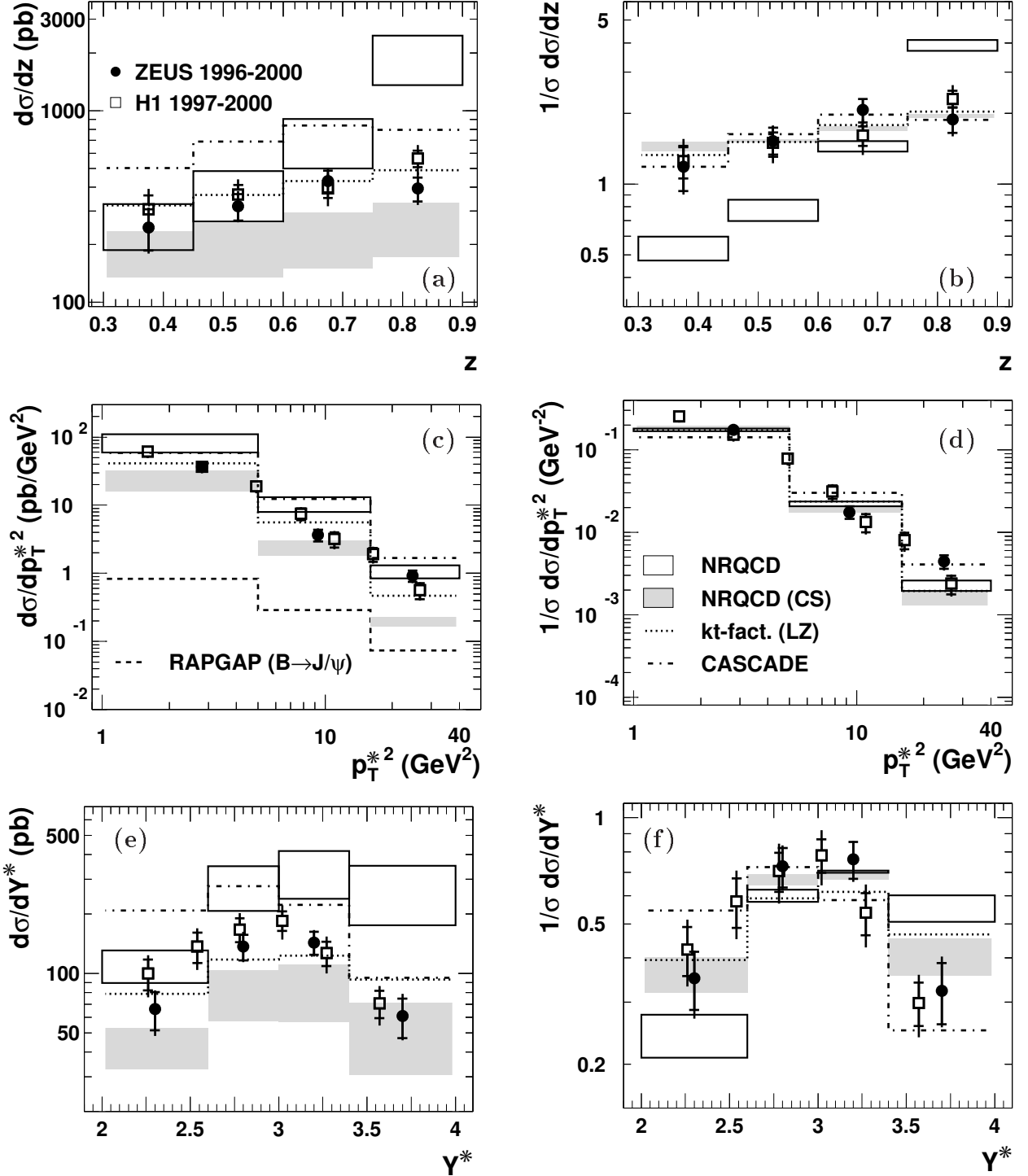
ZEUS

Figure 6: *Differential cross sections for the reaction $e\,p \rightarrow e\,J/\psi\,X$ in the kinematic region $2 < Q^2 < 100\,GeV^2$, $50 < W < 225\,GeV$, $0.3 < z < 0.9$ and $p_T^{*2} > 1\,GeV^2$ as a function of (a) z, (c) p_T^{*2} and (e) Y^*. The inner error bars of the data points show the statistical uncertainty; the outer bars show statistical and systematic uncertainties added in quadrature. The ZEUS and H1 data are compared to LO NRQCD predictions, a LO CS calculation, a prediction in the k_T-factorisation approach within the CSM and the CASCADE MC predictions. The H1 data points are plotted at the mean value of the data in each interval [14]. The ZEUS data for the p_T^{*2} differential cross section are plotted at the weighted mean, for each bin, of the EPJPSI MC prediction. (b), (d) and (f) show the data and the theoretical predictions normalised to unit area.*

23